

# RADIOMETRIC CALIBRATION OF FULL-WAVEFORM AIRBORNE LASER SCANNING DATA BASED ON NATURAL SURFACES

Hubert Lehner<sup>a</sup> and Christian Briese<sup>a,b</sup>

<sup>a</sup>Christian Doppler Laboratory, Institute of Photogrammetry and Remote Sensing,  
Vienna University of Technology, Gusshausstrasse 27-19, 1040 Vienna, Austria,  
(hl, cb)@ipf.tuwien.ac.at

<sup>b</sup>Ludwig Boltzmann Institute for Archaeological Prospection and Virtual Archaeology,  
Hohe Warte 38, 1190 Vienna, Austria

## Commission VII

**KEY WORDS:** Radiometry, Radiometric Calibration, LIDAR, Laser scanning

### ABSTRACT:

Airborne laser scanning (ALS) has become a commercially available and therefore widely used technique for obtaining the geometric structure of the earth's surface. For many ALS applications it is beneficial or even essential to classify the 3D point cloud into different categories (e.g. ground, vegetation, building). So far, most classification techniques use the geometry of the 3D point cloud or parameters which can be gained from analyzing the geometry or the number of echoes per emitted laser shot. Decomposing the echo waveform of full-waveform laser scanners provides in addition to the 3D position of each echo its amplitude and width. These physical observables are influenced by many different factors (e.g. range, angle of incidence, surface characteristics, atmosphere, etc.). Therefore, these attributes can hardly be used without radiometric calibration. In this paper the theory of the radar equation will be used to transform amplitude and echo width into radiometric calibration values, such as backscatter cross section, backscattering coefficients or incidence angle corrected versions of those. For this aim, external reference targets with known backscatter characteristics are necessary for the absolute radiometric calibration. In contrast to other approaches, this paper presents the usage of natural surfaces for this calibration task. These surfaces are observed in order to determine their backscatter characteristics independently from the ALS flight mission by a RIEGL reflectometer. Based on these observations the data of the ALS flight can be calibrated. Calibration results of data acquired by a RIEGL LMS-Q560 sensor are presented and discussed. Next to a strip-wise analysis, the radiometric calibration results of different strips in the overlapping region are studied. In this way, the accuracy of the calibration is analyzed (1) based on a very large area with approximately homogeneous backscatter characteristics, namely a parade yard, and (2) relatively by analyzing these overlapping regions.

## 1 INTRODUCTION

Airborne laser scanning (ALS, also referred to as airborne LIDAR (light detection and ranging)) is an active sampling method that is widely used for obtaining the geometric structure of the earth's surface. The resulting point cloud is a good basis for the modelling of the landscape for a variety of applications, e.g. hydrology (Mandlbürger et al., 2009), city modelling (Rottensteiner et al., 2007), forest mapping (Naesset, 1997, Hollaus et al., 2007), archaeology (Doneus et al., 2008). For these applications it is typically necessary to classify the ALS data into different classes (e.g. ground, vegetation, buildings). Most of the developed classification methods just rely on the geometric information provided by the acquired point cloud. However, with the introduction of small-footprint full-waveform (FWF) ALS sensors into the commercial market further additional attributes, i.e. the echo width and amplitude, for each echo can be determined. These attributes can be seen as physical observables that allow studying the radiometry of ALS data. However, in order to utilize this information a radiometric calibration of the ALS data is essential (Wagner et al., 2008b).

For the radiometric calibration of ALS data different methods were already published. Next to their mathematical or physical framework the approaches differ in the use of reference data. Some publications do not use reference surfaces at all and only try to compensate for specific influencing factors (Luzum et al., 2004, Donoghue et al., 2007, Höfle et al., 2007). Another group of authors rely on artificial reference targets that were placed within the area of interest during the data acquisition campaign

(Ahokas et al., 2006, Kaasalainen et al., 2007), while the third group of researchers tries to solve the radiometric calibration task with the usage of natural reference targets (Coren and Sterzai, 2006, Wagner et al., 2006, Briese et al., 2008).

Within this paper the practical application and validation of the radiometric calibration of small-footprint FWF-ALS data based on natural surface elements is presented and studied. The calibration procedure relies on the radar equation (Wagner et al., 2006) and on natural reference surfaces. These surfaces are observed in-situ by a RIEGL reflectometer (Briese et al., 2008). Based on these observations, the data of the ALS flight can be calibrated. In order to demonstrate the practical capability and to study the quality of the radiometric calibration this process is applied to an FWF-ALS data set acquired by a RIEGL LMS-Q560 sensor over the city of Vienna, Austria. Next to the practical application of the method the resulting calibrated data set is analysed strip-wise by a visual comparison of the radiometric information in the overlapping area of two strips. Furthermore, a quantitative comparison of the calibrated data sets is performed by an analysis of a difference model in the overlapping zone. Finally, after the discussion of the results, a short summary and an outlook into future research work conclude the paper.

## 2 RADIOMETRIC CALIBRATION

### 2.1 Theoretical Background

The basic relation between the transmitted power  $P_t$  and the received power  $P_r$  of an ALS system can be described by the LIDAR

adapted formulation of the radar equation (see equation 1), which considers all influencing factors: the receiver aperture diameter  $D_r$ , the range between sensor and target  $R$ , the laser beam divergence  $\beta_t$  and the backscatter cross section, as well as losses occurring due to the atmosphere or in the laser scanner system itself, i.e. a system and atmospheric transmission factor  $\eta_{sys}$  and  $\eta_{atm}$  respectively. The backscatter cross section combines all target parameters such as the size of the area illuminated by the laser beam  $A_i$ , the reflectivity  $\rho$  and the directionality of the scattering of the surface  $\Omega$  (Wagner et al., 2006, Briese et al., 2008, Jelalian, 1992):

$$P_r = \frac{P_t D_r^2}{4\pi R^4 \beta_t^2} \cdot \sigma \cdot \eta_{sys} \eta_{atm} \quad \text{with} \quad \sigma = \frac{4\pi}{\Omega} \rho A_i \quad (1)$$

Parameters which are unknown but can be assumed to be constant during one ALS campaign can be combined to one constant, the so-called calibration constant  $C_{cal}$ . Due to the fact that, in case of ALS systems with Gaussian system waveform, the received power is proportional to the product of the amplitude  $\hat{P}_i$  and the echo width  $s_{p,i}$ , it can be replaced by the term  $\hat{P}_i s_{p,i}$  (Wagner et al., 2006, Höfle et al., 2008). This yields the following form of the calibration equation for calculating the backscatter cross section  $\sigma$ :

$$\sigma = \frac{C_{cal} 4\pi R^4 \hat{P}_i s_{p,i}}{\eta_{atm}} \quad \text{with} \quad C_{cal} = \frac{\beta_t^2}{P_t D_r^2 \eta_{sys}} \quad (2)$$

The range, the amplitude and the echo width in equation 2 are results of the Gaussian decomposition of the full-waveform data, while the atmospheric transmission factor  $\eta_{atm}$  can be determined by meteorological data and radiative transfer models such as MODTRAN (Berk et al., 1998, Briese et al., 2008). In order to estimate the calibration constant in equation 2 only the backscatter cross section of a reference surface is necessary. This can be achieved by the second formula of equation 1, the assumption of a Lambertian scatterer, which means that the scattering solid angle  $\Omega$  is  $\pi$  steradians, and the knowledge of the reflectivity  $\rho$  of the reference surface. For a fast estimation the illuminated area  $A_i$  in equation 2 can be replaced by the laser footprint area at the scattering object  $A_{lf}$  (see figure 1 and equation 3).

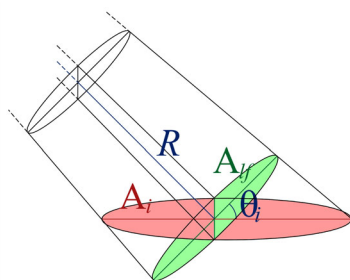


Figure 1: Laser footprint area at the scattering object  $A_{lf}$ , i.e. the circular area perpendicular to the laser beam at distance  $R$  (green area); area illuminated by the laser beam  $A_i$  at distance  $R$  and  $\theta_i$  angle of incidence (red area).

The laser footprint area at the scattering object (see green area in figure 1) can easily be calculated by the range  $R$  and the beam divergence  $\beta_t$ , while the area illuminated by the laser beam (see red area in figure 1) can be approximated by an ellipse whose calculation of the area additionally requires an estimation of the

local angle of incidence  $\theta_i$  (Lutz, 2003):

$$A_{lf} = \frac{\pi R^2 \beta_t^2}{4} \quad \text{resp.} \quad A_i = \frac{R^2 \beta_t^2 \pi}{4 \cos \theta_i} = \frac{A_{lf}}{\cos \theta_i} \quad (3)$$

Once the calibration constant is derived the calibrated backscatter cross sections of the individual echoes for the whole data set can be determined.

Due to different flight heights or beam divergence, the illuminated area  $A_i$  and therefore also the backscatter cross section  $\sigma$  can vary a lot. Therefore, Wagner et al. (2008a) introduce area-normalized values, so-called backscattering coefficients, which have the advantage that measurements with different resolution can be compared more easily. The backscatter cross section can be related to the illuminated area  $A_i$ , which leads to the cross section per unit-illuminated area  $\sigma^0$  [ $\text{m}^2 \text{m}^{-2}$ ] (Wagner et al., 2008b):

$$\sigma^0 = \frac{\sigma}{A_i} \quad (4)$$

Since the incidence angles change, it might be more convenient to normalize the backscatter cross section to the illuminated area at zero angle of incidence, i.e. the cross section of the incoming beam, which results in the so-called bistatic scattering coefficient  $\gamma$  [ $\text{m}^2 \text{m}^{-2}$ ] (Wagner et al., 2008b):

$$\gamma = \frac{\sigma}{A_{lf}} \quad (5)$$

The backscatter cross section  $\sigma$  as well as the backscattering coefficients  $\sigma^0$  and  $\gamma$  are not free from influences caused by the angle of incidence. In case of ideal Lambertian scatterers incidence angle corrected values can be achieved by division with the cosine of the local angle of incidence:

$$\sigma_\theta = \frac{\sigma}{\cos \theta_i} \quad \text{resp.} \quad \gamma_\theta = \frac{\gamma}{\cos \theta_i} \quad (6)$$

Although  $\sigma_0$  seems to be the most suitable value at first sight, it amplifies the effect of the angle of incidence (for an Lambertian scatterer by the square of the cosine law). The computational advantages of  $\gamma$  are obvious since no time-consuming local plane fits are necessary in order to estimate the local surface normal, which is required for the calculation of the local incidence angle. However, in case homogeneous values are aimed at for a homogeneous surface, incidence angle corrected values such as  $\sigma_\theta$  have to be computed. Since the estimation of the local surface normal can be uncertain or even impossible for some echoes, e.g. in vegetated areas, incidence angle corrected values cannot be guaranteed for the whole data set. Therefore, it depends on the subject of interest which calibration value to choose for further processing.

## 2.2 Practical Method

The practical method for radiometric calibration based on natural surfaces as reference targets is already presented in Briese et al. (2008). Therefore it will be mentioned only briefly. It consists of three parts (see figure 2).

Prior to the ALS flight natural reference targets should be selected in order to be able to measure the reflectivity by using the RIEGL reflectometer and Spectralon<sup>®</sup> diffuse reflectance standards (Labsphere Inc., 2010) at approximately the same time as the ALS data is acquired (see figure 2(a)) (Briese et al., 2008).

Meteorological data such as the visibility at the time of the flight either have to be observed during data acquisition or gained from

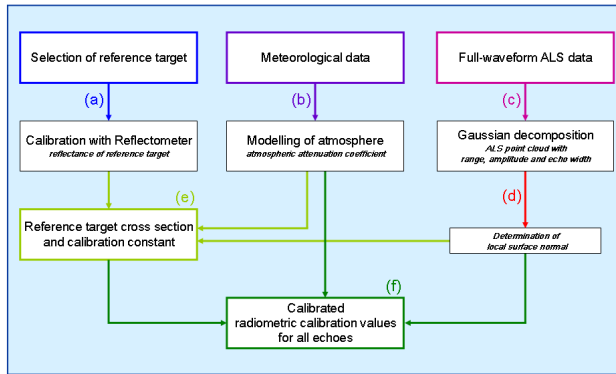


Figure 2: Operational workflow of radiometric calibration of full-waveform ALS data.

observation stations close to the campaign site afterwards. With the help of radiative transfer models an atmospheric attenuation coefficient can be derived (see figure 2(b)).

Decomposing the full-waveform data yields a 3D point cloud with additional information per echo such as range, amplitude and echo width (see figure 2(c)) (Wagner et al., 2006).

From here on the radiometric calibration is further processed by OPALS modules that were developed by the Institute of Photogrammetry and Remote Sensing (IPF) of the Vienna University of Technology (IPF, 2010). The `opalsImport` module is used to load the 3D point data with its attributes and its corresponding trajectory strip-wise into the OPALS data manager system for subsequent use in all OPALS modules dealing with point clouds. During the import process, `opalsImport` reconstructs the beam vector, echo number and number of returns of each echo and stores them as additional attributes in the data manager. Furthermore, the `opalsNormals` module performs a local plane fit for each point based on its neighbouring points in order to derive the local normal vector of each point. However, due to the partly high surface variation, it might not be possible to fit a plane for every echo (only planes with a maximal user specified tolerance value for the adjusted sigma value are accepted), e.g. in case of echoes originating from vegetation. Nevertheless, if the plane is accepted, the normalized normal vector is stored as additional attribute for each point in the data manager (see figure 2(d)).

In order to allow the radiometric calibration of ALS data the OPALS module `opalsRadioCal` was developed to firstly derive a mean calibration constant (see figure 2(e)). Within this step, for every echo within a given reference surface with given reflectivity and atmospheric attenuation coefficient the calibration constant is estimated according to the second formula in equation 1, the first formula in equation 2 and the formula displayed in equation 3. For points within the reference surface the local incidence angle is computed from the local normal vector and the beam vector. These calibration constants for each echo within a reference surface are used to determine a mean calibration constant for the whole ALS campaign. The `opalsRadioCal` module applies this mean calibration constant to secondly calculate the calibrated radiometric values for each echo. This process includes the estimation of the backscatter cross section, backscattering coefficients and incidence angle corrected values as mentioned in section 2.1 (see figure 2(f)).

### 3 RESULTS AND DISCUSSION

The radiometric calibration procedure was tested on a data subset of the Vienna wide ALS campaign carried out at the end of

2006 and beginning of 2007, namely on the parts of thirteen flight strips covering the area of the Schönbrunn palace, garden, zoo and surrounding living area. This particular full-waveform data set was acquired on the December 27<sup>th</sup> 2006, by the company Diamond Airborne Sensing GmbH with a RIEGL LMS-Q560, which operates at a wavelength of 1550 nm. The scan frequency was 200 kHz, the aircraft speed above ground 150 km/h, the flying height above ground 500 m and the scan angle  $\pm 30^\circ$ . These settings resulted in a swath overlap of about 60 %, a mean point density of more than 20 measurements per square meter and a laser footprint size on ground of about 25 cm. The meteorological data for modelling the atmosphere was received from three weather observation stations located within the city of Vienna.

Two smaller asphalt regions, one gravel region, one building roof and the big asphalt regions of the parade yard of the Maria Theresia casern in the south of the Schönbrunn gardens (see figure 3) were chosen as reference surfaces. Reflectances at zero angle of incidence between 15 % for one of the smaller asphalt regions up to 44 % for the gravel region were determined by the RIEGL reflectometer. For the parade yard in the centre of the three big buildings in figure 3 a reflectance of 23.5 % was measured.



Figure 3: RGB-Orthophoto of the Maria Theresia casern in the south of the Schönbrunn gardens (MA41, 2010).

The parade yard of the Maria Theresia casern in the south of the Schönbrunn gardens is by far the largest homogeneous area within the test site. Therefore, it was also used as reference surface during the calibration procedure. Additionally, this area enables to study the different radiometric calibration values, which can be seen in figure 4. The left diagram of figure 4(a) shows the selected echoes for the analysis of two overlapping flight strips, the echoes of the western strip ( $> 65\,000$ ) in green and echoes of the eastern one ( $> 113\,000$ ) in blue. In the eastern strip the parade yard is located close to the centre of the swath, while for the western strip it is located at the swath border. This can also be seen in the right diagram of figure 4(a), which shows range versus angle of incidence. The eastern echoes were acquired at angles of incidence up to  $22^\circ$  and the echoes of the western strip between  $18^\circ$  and  $30^\circ$ . With increasing incidence angles also the ranges increase, approximately up to 70 m. Hence, the effects which can be seen in the diagrams below combine the range and the angle of incidence dependencies. Figure 4(b) shows the original amplitude values versus range and versus angle of incidence. In both cases the decrease with increasing range and angle of in-



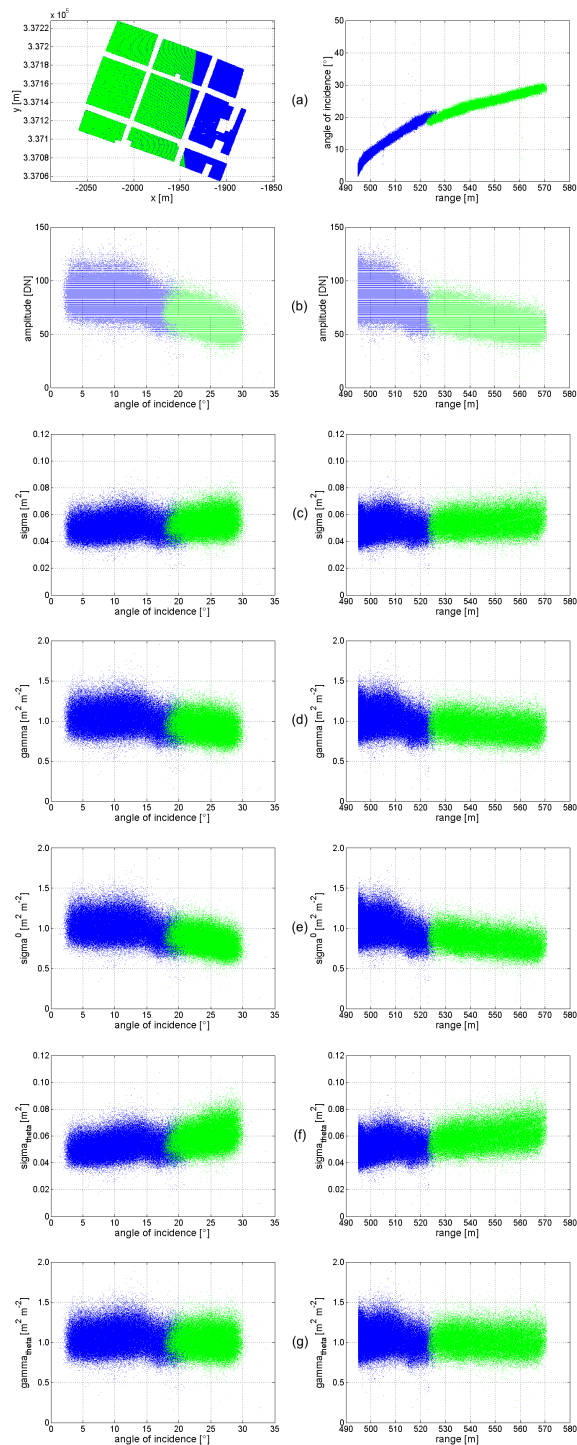


Figure 4: Colour-coded echoes of the parade yard of the Maria Theresia casern: points of western flight strip in green and points of eastern flight strip in blue. (a) coordinates of the echoes next to a diagram of range versus angle of incidence; (b) original amplitude measurements; (c) backscatter cross section  $\sigma$ ; (d) backscattering coefficient  $\gamma$ ; (e) backscattering coefficient  $\sigma^0$ ; (f) incidence angle corrected cross section  $\sigma_\theta$  and (g) incidence angle corrected backscattering coefficient  $\gamma_\theta$ . (b) – (g) specific value versus angle of incidence (left) and versus range (right).

idence can clearly be seen. Since the parade yard is a horizontal surface, the backscatter cross section  $\sigma$  (see figure 4(c)) already

shows homogeneous values for increasing range and angle of incidence. The backscattering coefficient  $\gamma$  (see figure 4(d)) shows a slight decrease, while  $\sigma^0$  (see figure 4(e)) shows a stronger decrease as expected. The incidence angle corrected value  $\sigma_\theta$  (see figure 4(f)) seems to overcorrect, while  $\gamma_\theta$  (see figure 4(g)) again delivers homogeneous values over the whole observed range and angle of incidence spectrum.

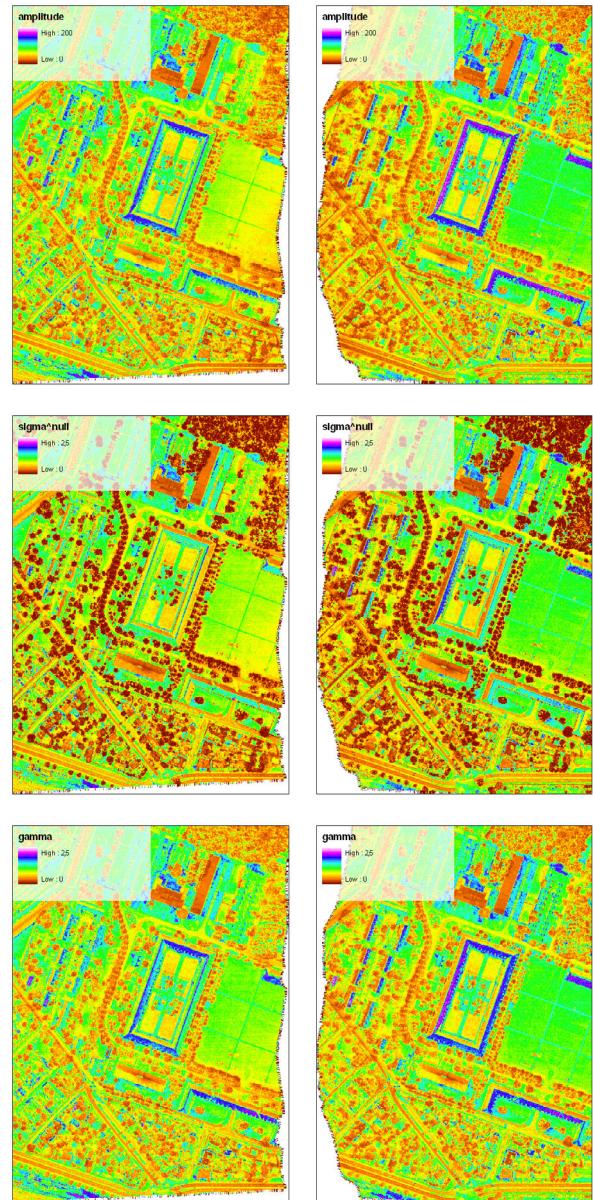


Figure 5: Colour-coded amplitude,  $\sigma^0$  and  $\gamma$  models of two flight strips for the overlapping region: (left) western flight strip and (right) eastern flight strip.

Figure 5 shows colour-coded amplitude,  $\sigma^0$  and  $\gamma$  models of two flight strips. Comparing the  $\sigma^0$  and  $\gamma$  images it can be seen that especially areas where the local normal estimation is critical, e.g. vegetated areas, yield significantly lower values. The roof areas of the big building in the centre of the western strip show unexpected values, which cannot be explained so far. The roof area with surface normals pointing towards the sensor and the area with normals pointing away, both of the eastern section of the building, show similar amplitude values instead of being significantly different. However, in the eastern strip the amplitudes behave like expected.



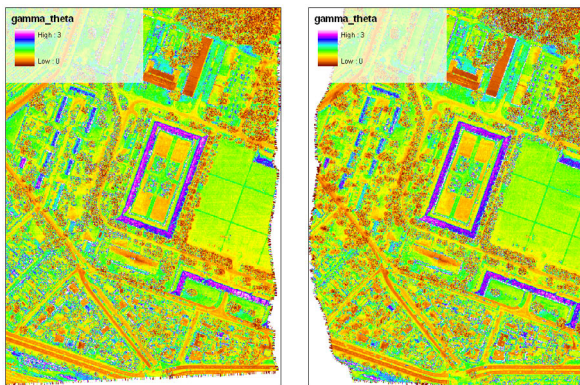


Figure 6: Colour-coded  $\gamma_\theta$  models of two flight strips for the overlapping region: (left) western flight strip and (right) eastern flight strip.

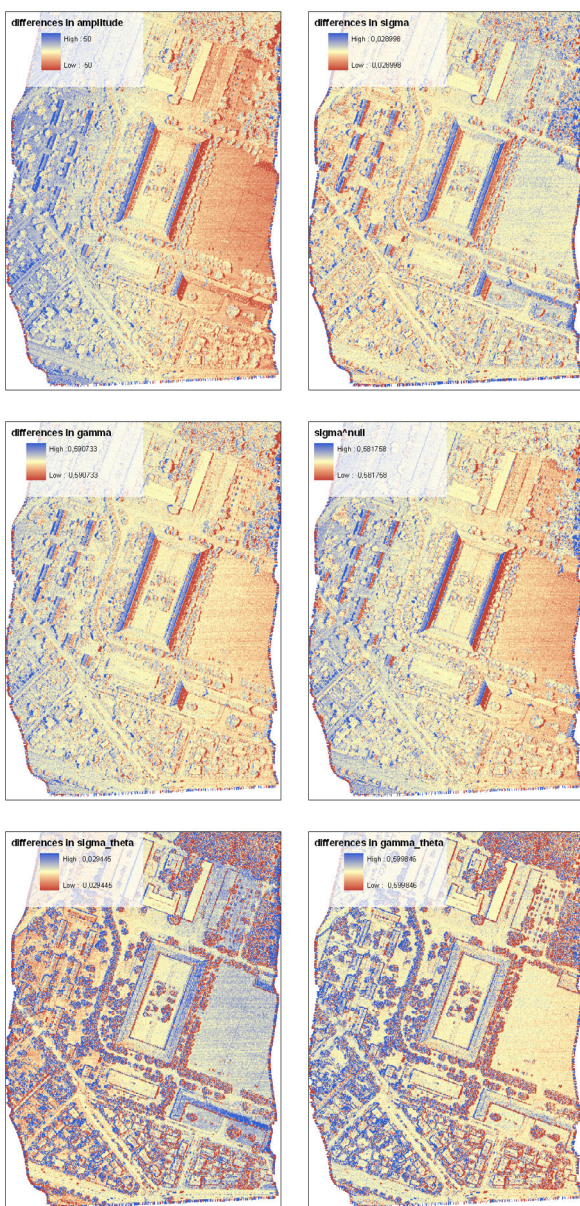


Figure 7: Colour-coded difference models of two overlapping flight strips for the original amplitude measurements and different radiometric calibration values.

The colour-coded incidence angle corrected  $\gamma_\theta$  model is displayed in figure 6. It can be seen, that the surfaces of the western and the eastern strip show similar values. However, within one strip roof areas with surface normals pointing towards the sensor and those with surface normals pointing away do not show similar values. This is unexpected but seems to be a result of the unexpected amplitude values as shown in figure 5.

In a next step, difference models of the different radiometric calibration values were calculated for the two overlapping flight strips (see figure 7). The colour-coded difference image of the amplitude values shows the expected increase in difference towards the borders of the overlapping swath. The differences in backscatter cross section  $\sigma$  already indicate similar values in the overlapping flight strips for wide regions, especially for horizontal surfaces. However, inclined roof surfaces still suffer from incidence angle effects. This can particularly be seen at the huge casern building in the centre of the difference image. The difference image of  $\gamma$  shows differences of the same strength as in the difference image of  $\sigma$ . The differences in  $\sigma^0$  between the overlapping strips on the other hand show again the amplification of the incidence angle dependence at the inclined roof surfaces. The incidence angle corrected values  $\sigma_\theta$  and  $\gamma_\theta$  strongly minimize the differences for roof areas. Since the incidence angles' estimation in vegetated areas is uncertain and sometimes impossible, this drawback can also be seen in the difference images of  $\sigma_\theta$  and  $\gamma_\theta$  by strong differences in either one or the other direction.

#### 4 CONCLUSION

This paper presents a comparison of different radiometric calibration values, the assets and drawbacks of each calibration value as well as a quantitative comparison by analyzing difference models of overlapping regions. The backscatter cross section  $\sigma$  delivers usable results especially for horizontal surfaces. However, area-normalized values should be the aim in case measurements with different resolution, e.g. acquired at significantly different flight heights over ground, with significantly different beam divergence and/or by different ALS sensors, shall be compared. Since  $\sigma_0$  proves to amplify the effect of the angle of incidence,  $\gamma$  turns out to be the preferred quantity of these so-called backscattering coefficients. Due to the fact that all these values still suffer from incidence angle dependencies, only incidence angle corrected values such as  $\sigma_\theta$  and  $\gamma_\theta$  are able to deliver homogeneous values for a homogeneous surface. Such values can only be derived for echoes, where the estimation of the local surface normal is successful, though. The analysis of the horizontal parade yard shows that  $\sigma_\theta$  tends to overcorrect the incidence angle dependence, while  $\gamma_\theta$  delivers homogeneous values for the homogeneously reflecting parade yard. Further evaluation has to be done especially concerning multi-temporal data, e.g. acquired by different sensors (e.g. with a different beam divergence, laser wavelength, etc.) and/or from different flight heights. Additionally, the unexpected behavior of the amplitude values that are visible in the upper left part of figure 5 (c.f. section 3) will be studied in the future.

#### ACKNOWLEDGEMENTS

We would like to thank Stadtvermessung Wien, Magistratsabteilung 41 (MA41, 2010), for providing the full-waveform ALS data, which was used for this study. Furthermore, we would like to thank the company Riegl Laser Measurement Systems GmbH (RIEGL, 2010) for the development of the reflectometer, a tool

which is essential for the proposed calibration method. This paper is a contribution to the EuroSDR project “Radiometric Calibration of ALS Intensity”. EuroSDR is a European spatial data research organisation (EuroSDR, 2010).

## REFERENCES

- Ahokas, E., Kaasalainen, S., Hyypä, J. and Suomalainen, J., 2006. Calibration of the Optech ALTM 3100 laser scanner intensity data using brightness targets. ISPRS Commission I Symposium “From Sensors to Imagery”, Paris, France, 2006 XXXVI, Part A1, pp. CD-ROM, T03–11.
- Berk, A., Bernstein, L. S., Anderson, G. P., Acharya, P. K., Robertson, D. C., Chetwynd, J. H. and Adler-Golden, S. M., 1998. Modtran cloud and multiple scattering upgrades with application to aviris. *Remote Sensing of Environment* 65(3), pp. 367–375.
- Briese, C., Höfle, B., Lehner, H., Wagner, W., Pfennigbauer, M. and Ullrich, A., 2008. Calibration of full-waveform airborne laser scanning data for object classification. In: M. D. Turner and G. W. Kamerman (eds), *Laser Radar Technology and Applications XIII, Proceedings of SPIE*, Vol. 6950, SPIE (International Society for Optical Engineering), SPIE Press, pp. 69500H–69500H–8. ISBN: 9780819471413 Defense and Security Symposium (17–20 March 2008, Orlando, Florida, USA).
- Coren, F. and Sterzai, P., 2006. Radiometric correction in laser scanning. *International Journal of Remote Sensing* 27(15), pp. 3097 – 3104.
- Doneus, M., Briese, C., Fera, M. and Janner, M., 2008. Archaeological prospection of forested areas using full-waveform airborne laser scanning. *Journal of Archaeological Science* 35(4), pp. 882–893.
- Donoghue, D., Watt, P., Cox, N. and Wilson, J., 2007. Remote sensing of species mixtures in conifer plantations using lidar height and intensity data. *Remote Sensing of Environment* 110(4), pp. 509–522.
- EuroSDR, 2010. EuroSDR - European Spatial Data Research Network. <http://www.eurohdr.net/>. vistet on 03/06/2010.
- Höfle, B., Geist, T., Rutzinger, M. and Pfeifer, N., 2007. Glacier surface segmentation using airborne laser scanning point cloud and intensity data. ISPRS WG III/3, III/4, V/3 VIII/11 Workshop “Laser Scanning 2007 and SilviLaser 2007”, Espoo, September 12–14, 2007, Finland Volume XXXVI, Part 3 / W52, pp. 195–200.
- Höfle, B., Hollaus, M., Lehner, H., Pfeifer, N. and Wagner, W., 2008. Area-based parameterization of forest structure using full-waveform airborne laser scanning data. In: R. Hill, J. Rosette and J. Surez (eds), *Proceedings of SilviLaser 2008: 8th international conference on LiDAR applications in forest assessment and inventory*, Heriot-Watt University, Edinburgh, UK, pp. 227–235. ISBN 978-0-85538-774-7.
- Hollaus, M., Wagner, W., Maier, B. and Schadauer, K., 2007. Airborne laser scanning of forest stem volume in a mountainous environment. *Sensors* 7(8), pp. 1559–1577.
- IPF, 2010. Institute of Photogrammetry and Remote Sensing (IPF) of the Vienna University of Technology, OPALS - Orientation and Processing of Airborne Laser Scanning data. [http://www.ipf.tuwien.ac.at/opals/opals\\_docu/index.html](http://www.ipf.tuwien.ac.at/opals/opals_docu/index.html). vistet on 03/06/2010.
- Jelalian, A. V., 1992. *Laser Radar Systems*. Artech House, Boston London. ISBN: 978-0890065549.
- Kaasalainen, S., Hyypä, J., Litkey, P., Hyypä, H., Ahokas, E., Kukko, A. and Kaartinen, H., 2007. Radiometric calibration of als intensity. ISPRS WG III/3, III/4, V/3 VIII/11 Workshop “Laser Scanning 2007 and SilviLaser 2007”, Espoo, September 12–14, 2007, Finland Volume XXXVI, Part 3 / W52, pp. 201–205.
- Labsphere Inc., 2010. Spectralon - Diffuse Reflectance Standards. [http://www.labsphere.com/data/userFiles/DiffuseReflectanceStandardsProductSheet\\_7.pdf](http://www.labsphere.com/data/userFiles/DiffuseReflectanceStandardsProductSheet_7.pdf). vistet on 03/06/2010.
- Lutz, E. R., 2003. Investigations of airborne laser scanning signal intensity on glacial surfaces - utilizing comprehensive laser geometry modeling and surface type modeling (a case study: Svar-tisheibreen, norway). Master’s thesis, Institut für Geographie der Leopold-Franzens-Universitt Innsbruck.
- Luzum, B., Starek, M. and Slatton, K. C., 2004. Normalizing alsm intensities. Center Report Rep.2004-07-001, Geosensing Engineering and Mapping (GEM), Civil and Coastal Engineering Department, University of Florida.
- MA41, 2010. Stadtvermessung Wien, Magistratsabteilung 41. <http://www.wien.gv.at/stadtentwicklung/stadtvermessung/index.html>. vistet on 03/06/2010.
- Mandlbürger, G., Hauer, C., Höfle, B., Habersack, H. and Pfeifer, N., 2009. Optimisation of lidar derived terrain models for river flow modelling. *Hydrology and Earth System Sciences* 13, pp. 1453–1466.
- Naesset, E., 1997. Estimating timber volume of forest stands using airborne laser scanner data. *Remote Sensing of Environment* 61(2), pp. 246–253.
- RIEGL, 2010. Riegl Laser Measurement Systems GmbH. <http://www.riegl.com/>. vistet on 03/06/2010.
- Rottensteiner, F., Trinder, J., Clode, S. and Kubik, K., 2007. Building detection by fusion of airborne laser scanner data and multi-spectral images: Performance evaluation and sensitivity analysis. *ISPRS Journal of Photogrammetry and Remote Sensing* 62(2), pp. 135–149.
- Wagner, W., Hollaus, M., Briese, C. and Ducic, V., 2008a. 3d vegetation mapping using small-footprint full-waveform airborne laser scanners. *International Journal of Remote Sensing* 29(5), pp. 1433–1452.
- Wagner, W., Hyypä, J., Ullrich, A., Lehner, H., Briese, C. and Kaasalainen, S., 2008b. Radiometric calibration of full-waveform small-footprint airborne laser scanners. ISPRS XXI ISPRS Congress, Commission I, WG I/2, July 3–11, 2008, Beijing, China XXXVII, Part B1, pp. 163–168. ISSN 1682-1750.
- Wagner, W., Ullrich, A., Ducic, V., Melzer, T. and Studnicka, N., 2006. Gaussian decomposition and calibration of a novel small-footprint full-waveform digitising airborne laser scanner. *ISPRS Journal of Photogrammetry and Remote Sensing* 60(2), pp. 100–112.